

Asymptotic and numerical studies of the Becker-Döring model for transient homogeneous nucleation

L. L. Bonilla[*]

*Escuela Politécnica Superior, Universidad Carlos III de Madrid,
Avda. Universidad 30, E-28911 Leganés, Spain*

A. Carpio[†]

*Departamento de Matemática Aplicada,
Universidad Complutense de Madrid, E-28040 Madrid, Spain*

Y. Farjoun[‡] and J. C. Neu[◇]

Department of Mathematics, University of California at Berkeley, Berkeley, CA 94720, USA

(Dated: October 2, 2018)

Abstract

Transient homogeneous nucleation is studied in the limit of large critical sizes. Starting from pure monomers, three eras of transient nucleation are characterized in the classic Becker-Döring kinetic equations with the Turnbull-Fisher discrete diffusivity. After an initial stage in which the number of monomers decreases, many clusters of small size are produced and a continuous size distribution is created. During the second era, nuclei are increasing steadily in size in such a way that their distribution appears as a wave front advancing towards the critical size for steady nucleation. The nucleation rate at critical size is negligible during this era. After the wave front reaches critical size, it ignites the creation of supercritical clusters at a rate that increases monotonically until its steady value is reached. Analytical formulas for the transient nucleation rate and the time lag are obtained that improve classical ones and compare very well with direct numerical solutions. In addition, we propose and solve numerically a modified Becker-Döring model having a discrete diffusivity proportional to the area of a spherical cluster with k monomers for small k (as in the Turnbull-Fisher case) and to the cluster radius for large k (as in the case of diffusive growth of clusters).

Key words: Kinetics of first order phase transitions; homogeneous nucleation; Becker-Döring equations; singular perturbation; asymptotic theory.

AMS subject classifications. 82C20; 82C26; 34E15.

PACS numbers:

I. INTRODUCTION

In first order phase transitions, it is possible to achieve that the system is in a metastable phase for values of the control parameter at which another phase is stable. Then nuclei of the stable phase appear at random locations and they typically grow or decay depending on whether their size surpasses a critical size [1]. In homogeneous nucleation processes, the probability density of finding a cluster of the stable phase with k monomers does not depend on the position. Homogeneous nucleation occurs in many examples of first order phase transitions, such as condensation of liquid droplets from a supersaturated vapor, glass-to-crystal transformations [2], crystal nucleation in undercooled liquids [3], and in polymers [4], growth of spherical aggregates beyond the critical micelle concentration (CMC) [5, 6], precipitation processes [7] and the segregation by coarsening of binary alloys quenched into the miscibility gap [4, 8]. In condensed systems, the time needed for the nucleation rate of supercritical clusters to reach a stationary value is large, which facilitates their theoretical and experimental study [3]. Authoritative reviews of nucleation in condensed systems are due to Wu [9] for theory, analytical and numerical methods, and to Kelton [3], who is not always reliable in his assessment of theories, but included a wealth of very valuable experimental data.

While nucleation is a random process, the cluster size distribution function satisfies deterministic equations which are particular cases of coagulation-fragmentation equations [10]. Typically, we assume that a cluster can grow or decay by adding or shedding one monomer at a time. Then homogeneous nucleation is described by the Becker-Döring (BD) discrete kinetic equations [3, 11]. Suppose that nucleation occurs in a lattice in which there are many more binding sites, M , than particles, N , [6, 12]. We shall consider the thermodynamic limit, $N \rightarrow \infty$ with fixed particle density per site, $\rho \equiv N/M$. Let p_k be the number of clusters with k particles or, in short, k clusters, and let $\rho_k \equiv p_k/M$ be the density of k clusters. Note that the number densities per site, ρ and ρ_k , are both dimensionless. Number densities per unit volume are obtained dividing ρ and ρ_k by the molecular volume, $v = V/M$. The BD equations (BDE) are [6]

$$\dot{\rho}_k = j_{k-1} - j_k \equiv -D_- j_k, \quad k \geq 2, \quad (1)$$

$$j_k = d_k \left\{ e^{\frac{D_+ \varepsilon_k}{k_B T}} \rho_1 \rho_k - \rho_{k+1} \right\}. \quad (2)$$

In (2), ε_k is the binding energy of a k cluster, required to separate it into its monomer components. For spherical aggregates,

$$\varepsilon_k = \left((k-1)\alpha - \frac{3}{2}\sigma(k^{\frac{2}{3}} - 1) \right) k_B T. \quad (3)$$

This formula holds for $k \gg 1$, but we shall use it for all $k \geq 1$. $\alpha k_B T$ is the monomer-monomer bonding energy [5] which, in the case of precipitation of crystals from a solution or segregation by coarsening of binary alloys, may depend on the particle density ρ (volume fraction) through some empirical formulas [11]. In Eq. (3), $\sigma = 2\gamma_s(4\pi v^2/3)^{\frac{1}{3}}/(k_B T)$, where γ_s and $v = V/M$ are the interfacial free energy per unit area (surface tension) and the molecular volume, respectively. Note that α and σ are both dimensionless. The correction $3\sigma k_B T/2$ in (3) ensures that $\varepsilon_1 = 0$, and it improves the agreement between the nucleation rate obtained from the BDE and experiments [9]. More precise atomic models were proposed by Penrose et al [11].

The monomer density ρ_1 can be obtained from the conservation identity

$$\sum_{k=1}^{\infty} k \rho_k = \rho, \quad (4)$$

in which the total particle density ρ is constant. In (1), $\dot{\rho}_k = d\rho_k/dt$ and $D_{\pm}u_k \equiv \pm[u_{k\pm 1} - u_k]$ are finite differences. The time t , the discrete diffusivity d_k and the flux j_k are nondimensional. t and d_k are related to the dimensional time t^* and decay coefficient d_k^* as follows [12]

$$t = \Omega t^*, \quad d_k = \frac{d_k^*}{\Omega}. \quad (5)$$

Here the factor Ω has units of frequency, it depends on the particular model we choose for d_k , and is determined in Appendix A for the Turnbull-Fisher (TF) kinetics (which assumes that a monomer has to overcome an activation energy barrier for its transfer across the interface of a cluster). The TF d_k is

$$d_k = k^{2/3} e^{D+g_k/2}, \quad \Omega = \frac{12D_0 e^{-Q/(RT)}}{v^{2/3}}. \quad (6)$$

Here $D = D_0 e^{-Q/(RT)}$ is the diffusion coefficient in the liquid, Q is the activation energy for diffusion, $R = k_B N_A$ is the gas constant and v is the molecular volume. In the classical theory, d_k is proportional to the surface area of a k cluster. In other models, d_k is selected

so as to yield the known expression for the adiabatic growth of a nucleus of critical size by diffusion [7] or by heat transfer [12]. The discrete diffusivity of these later models is proportional to the cluster radius, thereby to $k^{1/3}$.

The flux j_k in size space is the net rate of creation of a $k + 1$ cluster from a k cluster, given by the mass action law. Notice that we have selected the kinetic coefficient for monomer aggregation to d_k , the coefficient for decay of a $(k + 1)$ cluster, so that

$$\tilde{\rho}_k = \rho_1^k \exp\left(\frac{\varepsilon_k}{k_B T}\right). \quad (7)$$

is the equilibrium size distribution solving $j_k = 0$. This is the detailed balance assumption whose validity is discussed in Wu's review [9].

Eqs. (1), (2), (3), (4) and (6) form a closed system of equations that we can solve for an appropriate initial condition. If initially only monomers are present, we have $\rho_1(0) = \rho$, and $\rho_k(0) = 0$ for $k \geq 2$. The stationary solutions of the BDE and the phenomenon of phase segregation [13] will be described below in Section II. In Section III, we shall solve numerically the BDE for parameter corresponding to the glass-crystal transition in disilicate glasses [3] and explain the results by means of an asymptotic theory valid for large critical size. A more detailed version of the material in Sections II and III of the present paper can be found in Ref. [12] which, in addition, contains a model for the kinetic constant d_k based on thermal diffusion, not on activation processes as the TF model. The asymptotic theory for the discrete BDE is essentially the same for both models of the constant d_k . Most previous asymptotic theories correspond to the continuum limit of the BDE which is a parabolic partial differential equation known as the Zeldovich-Frenkel equation (ZFE) [9], and thus differ from and are less precise than ours [12].

A somewhat puzzling point in nucleation theory is that the growth of a k cluster is proportional to its surface area (therefore to $k^{2/3}$) if we assume that capture or emission of a monomer is an activated process as in the TF model. However, clusters are supposed to grow by diffusion (and thus at a rate proportional to $k^{1/3}$) after nucleation has stopped and coarsening begins [14]. In Section IV of the present paper, we present a new modified BD model such that the growth of a cluster is proportional to $k^{2/3}$ for small size k (as in the TF model) and to $k^{1/3}$ (as for the diffusive growth of precipitates) if k is large. We discuss briefly the results obtained with these two models and their relation to other studies in the literature.

II. BDE AND THEIR STATIONARY SOLUTIONS

A. Equilibrium size distribution

The equilibrium distribution (7) satisfies $j_k = 0$ and it can be written as

$$\tilde{\rho}_k = \rho_1 e^{-g_k}, \quad (8)$$

where g_k is the *activation energy* given by

$$g_k = \sigma_k - (k-1)\varphi, \quad \sigma_k = \frac{3}{2}\sigma(k^{\frac{2}{3}} - 1), \quad (k \geq 1), \quad \varphi = \ln(e^\alpha \rho_1). \quad (9)$$

Here $\sigma_1 = 0 = g_1$. Assuming $k \gg 1$, g_k achieves its global maximum $g_m = \sigma k_c^{2/3}/2 + \sigma k_c^{-1/3} - 3\sigma/2$ at the critical size

$$k = k_c \equiv \left(\frac{\sigma}{\varphi}\right)^3. \quad (10)$$

Rewriting the flux (2) in the BDEs in terms of the activation energy, we obtain

$$j_k = d_k \left\{ (e^{-D+g_k} - 1) \rho_k - D_+ \rho_k \right\}. \quad (11)$$

Eq. (1) is a spatially discrete Smoluchowski equation with diffusion coefficient d_k and drift velocity

$$v_k = d_k (e^{-D+g_k} - 1). \quad (12)$$

Notice that $v_k < 0$ for $k < k_c$ (subcritical clusters shrink) and $v_k > 0$ for $k > k_c$ (supercritical clusters grow).

For the equilibrium densities (8), the conservation identity (4) becomes

$$e^\alpha \rho = \sum_{k=1}^{\infty} k (e^\alpha \rho_1)^k e^{-\sigma_k} = \sum_{k=1}^{\infty} k e^{k\varphi - \sigma_k}. \quad (13)$$

This series converges for $e^\alpha \rho_1 = e^\varphi \leq 1$ ($\varphi \leq 0$), and diverges for $e^\alpha \rho_1 > 1$ ($\varphi > 0$). At the critical micelle concentration (CMC), $\rho_1 = e^{-\alpha}$ ($\varphi = 0$), we obtain the critical density above which equilibrium is no longer possible,

$$e^\alpha \rho_c = 1 + \sum_{k=2}^{\infty} k e^{-\sigma_k}. \quad (14)$$

For $\rho > \rho_c$, the BD kinetic equations predict phase segregation, i.e., indefinite growth of ever larger clusters, and there remains a residual monomer concentration whose density $\rho_1 e^\alpha \rightarrow 1$ as $t \rightarrow \infty$ [12, 13, 14].

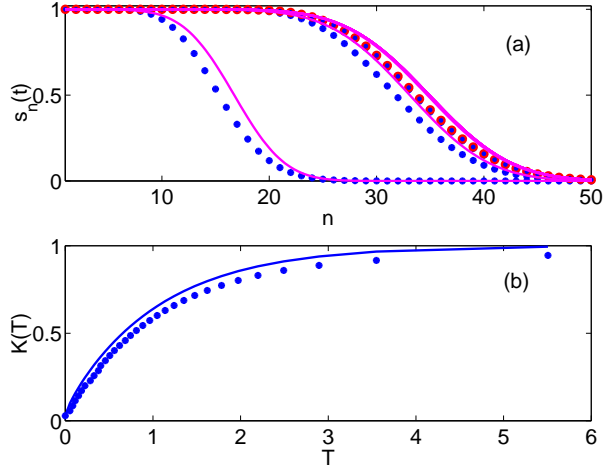


FIG. 1: (a) Comparison of $s_n(t)$ evaluated (at different times) from the numerical solution of the discrete equations (23) to the asymptotic result (40) (solid line). (b) $K(T)$ calculated from Eq. (31) with $K(0) = \epsilon^3$ (solid line) is compared to the numerically obtained position of the wave front. Data correspond to disilicate glass at 820 K. All variables are written in dimensionless units.

B. The controlling parameters

The simplest nucleation problem consists of solving the BD equations (4), (1) and (11), with dimensionless activation energy $g_k = \sigma_k - (k-1)\varphi$, discrete diffusivity d_k (to be chosen later) and initial conditions

$$\rho_1(0) = \rho, \quad \rho_2(0) = \rho_3(0) = \dots = 0. \quad (15)$$

The only parameters left in this initial value problem are ρ and σ . ρ controls the long-time behavior of the BDE: If $\rho \leq \rho_c$ given by (14), $\rho_k(t)$ approach their equilibrium values (8), with monomer density ρ_1 that solves Equation (4). If $\rho > \rho_c$, cluster sizes grow indefinitely whereas their density becomes small.

Let us identify the controlling parameters ρ and σ in a physical system undergoing homogeneous nucleation. A good experimental example for which abundant data exist is the transformation of lithium disilicate glasses to crystals (devitrification) [3]. In disilicate, the free energy per molecule of the crystal phase in the activation energy (9) is proportional to

the undercooling

$$\tilde{\varphi} = \frac{\Delta S_f(T_m - T)}{N_A k_B T}, \quad (16)$$

where T_m is the melting temperature, ΔS_f is the molar entropy of fusion and N_A is Avogadro's number; see the parameter values in Table I [2]. The dimensionless density $\rho = e^{\varphi(0) - \alpha}$ can be extracted from Eq. (16) as explained in Section III. In energy units, the activation free energy is $k_B T g_k = \gamma_s 4\pi a^2 - k_B T \varphi k$, where $a = [3v/(4\pi)]^{1/3} k^{1/3}$ is the radius of a spherical k cluster. Thus

$$k_B T \left(g_k - \varphi + \frac{3\sigma}{2} \right) = \gamma_s (4\pi)^{1/3} (3v)^{2/3} k^{2/3} - \Delta S_f (T_m - T) k / N_A. \quad (17)$$

Comparing (17) with (9) yields $\sigma = (32\pi v^2/3)^{1/3} \gamma_s / (k_B T)$, and the critical size

$$k_c^{1/3} = \left(\frac{32\pi v^2}{3} \right)^{1/3} \frac{\gamma_s N_A}{\Delta S_f (T_m - T)} = \frac{\sigma}{\tilde{\varphi}}. \quad (18)$$

The other parameters in Table I will be used later to model the discrete diffusivity in the BDE. We observe that the critical size increases with temperature: $k_c = 18$ at 703 K and $k_c = 34$ at 820 K. For other materials, such as undercooled liquid metals, critical sizes can be rather large: liquid iron at maximum undercooling has $k_c = 494$, whereas $k_c = 2253$ for liquid rutenium at maximum undercooling [3].

C. Equivalent Becker-Döring system

As they stand, the BDE are rather stiff and hard to solve numerically [12]. This motivates the following change of variable

$$\rho_k = \rho_1 e^{-g_k} s_k = e^{-\alpha} e^{k\varphi - \sigma_k} s_k, \quad (19)$$

according to (9). Note that $s_k = 1$ in equilibrium. Since $g_1 = 0$, this equation implies

$$s_1 \equiv 1, \quad (20)$$

for all t . For the initial condition (15), $e^{\varphi(0) - \alpha} = \rho_1(0) = \rho$, and the conservation identity (4) becomes

$$e^{\varphi(0)} = e^\varphi + \sum_{k=2}^{\infty} k e^{k\varphi - \sigma_k} s_k, \quad (21)$$

Parameter	Symbol	Value
Melting temperature	T_m	1300 K
Entropy of fusion	ΔS_f	40 J mol ⁻¹ K ⁻¹
Surface tension	γ_s	0.15 J/m ²
Preexponential diffusivity	D_0	2×10^9 m ² s ⁻¹
Activation energy for diffusion	Q	440 kJ/mol
Molecular volume	v	10^{-28} m ³
TF time scale (703K)	Ω^{-1}	1.226 hours
Critical size (703K)	k_c	18
Undercooling (703K)	$\tilde{\varphi}$	4.087
Dimensionless surface tension (703K)	σ	10.74
Dimensionless free energy barrier (703K)	$g_m = \frac{\sigma}{2}k_c^{2/3} - \frac{3\sigma}{2} + \tilde{\varphi}$	25.177

TABLE I: Data for lithium disilicate glass

in which we have used (19). In terms of the s_k , the flux can be written as

$$e^\alpha j_k = d_k \exp[(k+1)\varphi - \sigma_{k+1}] (s_k - s_{k+1}), \quad (22)$$

and the BDE (1) and (11) become

$$\dot{s}_k + u_k(s_{k+1} - s_k) = -k\dot{\varphi}s_k + d_{k-1}(s_{k-1} - 2s_k + s_{k+1}), \quad (23)$$

for $k \geq 2$. Here,

$$u_k = d_{k-1} - d_k e^{\varphi - D_+ \sigma_k}. \quad (24)$$

The term $u_k D_+ s_k$ in Eq. (23) represents *discrete advection*, with a drift velocity $u_k = -v_k + (d_{k-1} - d_k) \sim -v_k$, which is essentially minus the drift velocity in the original BDE for $k \gg 1$. Thus, the advection in Eq. (23) *climbs up* the activation energy barrier, from small values of g_k to large ones.

In summary, the transformed nucleation initial-boundary value problem consists of the balance equations (23), the particle conservation equation (21), the boundary condition (20), $s_1 = 1$, and initial conditions $s_k(0) = 0$ for all $k \geq 2$. Its solution gives $\varphi(t)$ and $s_k(t)$ for all $k \geq 2$ and all $t > 0$.

D. Stationary solution

The stationary solution of the BDE has a flux independent of cluster size, so that $e^\alpha j_k = d_k \exp[(k+1)\varphi - \sigma_{k+1}] (s_k - s_{k+1}) = j$, from which $(s_{k+1} - s_k) = -j \exp[\sigma_{k+1} - (k+1)\varphi]/d_k$, and therefore

$$s_k = 1 - j \sum_{l=1}^{k-1} \frac{\exp[\sigma_{l+1} - (l+1)\varphi]}{d_l}, \quad (25)$$

for $k \geq 2$. Since $s_\infty = 0$, j can be obtained from this expression in terms of an infinite series

$$j = \frac{1}{\sum_{l=1}^{\infty} \exp[\sigma_{l+1} - (l+1)\varphi - \ln d_l]}. \quad (26)$$

Substituting back this expression into (25), we obtain

$$s_k = 1 - \frac{\sum_{l=1}^{k-1} \exp[\sigma_{l+1} - (l+1)\varphi - \ln d_l]}{\sum_{l=1}^{\infty} \exp[\sigma_{l+1} - (l+1)\varphi - \ln d_l]}. \quad (27)$$

Then, $\rho_k = \rho_1 e^{-gk} s_k$.

III. ASYMPTOTIC THEORY OF NUCLEATION

In this section, we shall interpret the numerical solutions shown in Figures 1 and 2 by using singular perturbation methods. Starting from pure monomers, the numerical solution of the BDE show that there are three well differentiated stages or eras of transient nucleation. After an initial stage in which the number of monomers ρ_1 decreases, many clusters of small size are produced and a continuous size distribution is created. During the second era, nuclei are increasing steadily in size in such a way that their continuum size distribution appears as a wave front advancing towards the critical size for stationary nucleation; see Fig. 1. The nucleation rate at critical size is negligible during this second era. After the wave front reaches critical size, it ignites the creation of supercritical clusters at a rate that increases monotonically until its steady value is reached; see Fig. 2. Our asymptotic theory of the BDE will be described using the TF discrete diffusivity (6) and compared to numerical solution of the BDE for the crystallization of disilicate glass at different undercoolings.

A. Initial transient

Initially, $\rho_1(0) = \rho$ and there are no multiparticle aggregates. There is an initial transient stage during which dimers, trimers, etc. form at the expense of the monomers. This initial

stage is characterized by the decay of the chemical driving force $\varphi = \alpha + \ln \rho_1$ to a quasi-stationary value $\tilde{\varphi}$, given by Eq. (16) in the case of disilicate glass, and the emergence of a continuum size distribution. Knowing this, *we choose the initial chemical driving force $\varphi(0)$ so that the quasistationary value $\tilde{\varphi}$ given by Eq. (16) is attained at the end of the initial stage.*

In materials such as disilicate glass at the temperatures we consider, the critical size is relatively small. Then $\varphi(0) \approx \tilde{\varphi}$, and the initial stage is very short. As the critical size increases (as in the case of undercooled liquid metals), $\varphi(0)$ may differ appreciably from $\tilde{\varphi}$, and the initial stage lasts longer. However, even in such cases, the duration of the initial stage compared to the duration of the overall transient to stationary nucleation is of order $k_c^{-2/3} \ll 1$ [12].

B. Wave front advancing towards the cluster of critical size

After the first era, clusters of increasing size are formed. For sufficiently small clusters, the continuum size distribution approaches the equilibrium distribution with $\varphi = \tilde{\varphi}$. This situation can be observed as an advancing wave front in the variable $s_k(t)$, satisfying $s_k \sim 1$ (equilibrium) behind the front and $s_k \sim 0$ ahead of the front. This second era is described by Equations (21) to (24) with $\varphi = \tilde{\varphi}$ and $\dot{\varphi} = 0$. The critical sizes (18) for disilicate glass are relatively small, between 10 and 50, but they are large for undercooled liquid metals, generally between 100 and 1000. Hence we shall use $k_c^{-1/3}$ as a small gauge parameter

$$\epsilon = \frac{\tilde{\varphi}}{\sigma}. \quad (28)$$

Our asymptotic analysis will be carried out in the limit $\epsilon \rightarrow 0$, and therefore $k_c = \epsilon^{-3} \rightarrow \infty$. Then d_k , u_k and σ_k in Eqs. (6), (23) and (24) are smooth functions of $k > 0$:

$$d(k) = k^{2/3} e^{[D + \sigma(k) - \tilde{\varphi}]/2}, \quad \sigma(k) = \frac{3}{2}\sigma(k^{2/3} - 1), \quad (29)$$

$$u(k) = d(k-1) - d(k) \exp[\tilde{\varphi} - \sigma(k+1) + \sigma(k)]. \quad (30)$$

1. Position of the wave front

In the numerical solutions shown in Fig. 1(a), the graphs of s_k vs. k at fixed time have clear inflection points at some k , where $s_k \approx 1/2$. The inflection point is taken as the

position of the wave front. In the continuum model, the front position $k = k_f(t)$ is a smooth function which obeys $\dot{k}_f = u(k_f)$. If we scale $k_f = K/\epsilon^3$, this equation becomes

$$\frac{dK}{dT} = U(K), \quad T = \epsilon t, \quad (31)$$

$$U(K) \equiv \lim_{\epsilon \rightarrow 0} [\epsilon^2 u(\epsilon^{-3}K)] = 2K^{2/3} \sinh\left(\frac{\tilde{\varphi}}{2}(K^{-1/3} - 1)\right), \quad (32)$$

in the limit as $\epsilon \rightarrow 0$. Fig. 1(b) compares the wave front position calculated by solving (31) with $K(0) = \epsilon^3$ to the numerical solution of (23). Note that the solution of (31) presents a time shift with respect to the numerical solution of the discrete model. This time shift reflects the breakdown of the continuum limit as $K \rightarrow 0$, due to discreteness, and also the transient in $\varphi(t)$ before it settles to $\tilde{\varphi}$. If the solution of Eq. (31) - (32) is forced to agree with the numerical $K(T)$ when the latter is, say, 0.1, the comparison fares much better.

2. Shape of the wave front

The leading edge of the wave front is a layer centered at $K(T)$ in which s_k decreases from 1 to 0 as k increases through it. The continuum representation of s_k in this layer is

$$s_k = S(X, T; \epsilon), \quad X = \epsilon^{3/2} \left(k - \frac{K}{\epsilon^3}\right). \quad (33)$$

Inserting (33) into (23), and then using (31), we obtain

$$\frac{\partial S}{\partial T} + U'(K)X \frac{\partial S}{\partial X} = D(K) \frac{\partial^2 S}{\partial X^2}, \quad (34)$$

$$D(K) \equiv \lim_{\epsilon \rightarrow 0} \left[d(\epsilon^{-3}K) - \frac{1}{2} u(\epsilon^{-3}K) \right] \epsilon^2 = K^{2/3} \cosh\left(\frac{\tilde{\varphi}}{2}(K^{-1/3} - 1)\right), \quad (35)$$

in the limit as $\epsilon \rightarrow 0$. Had we carried out the same analysis for the ZFE, we would have found $D(K) \sim d(\epsilon^{-3}K)\epsilon$. This would have resulted in a wider wave front and a longer time to ignition than those described below.

3. Flux and wave front width

Besides determining the shape of the wave front near its location, Eq. (34) yields the behavior of the flux (creation rate of clusters larger than k) j_k near $k = k_f$. If we substitute (6) and (33) into (22), we obtain

$$j_k \sim \epsilon^{-1/2} K^{2/3} e^{3\tilde{\varphi}/(2\epsilon)} \exp\left[-\frac{G(K)}{\epsilon^3} - \frac{G'(K)X}{\epsilon^{3/2}} - \frac{G'(K)}{2} - \frac{G''(K)}{2} X^2\right] \frac{\partial S}{\partial X}. \quad (36)$$

Here, $G(K) \equiv \tilde{\varphi} \left(\frac{3}{2}K^{2/3} - K \right)$ is a scaled version of the activation energy (9).

Since j_k is proportional to $\partial S/\partial X$, it is convenient to differentiate (34) with respect to X in order to obtain an equation for $J \equiv -\partial S/\partial X$,

$$\frac{\partial J}{\partial T} + U'(K) \frac{\partial(X J)}{\partial X} = D(K) \frac{\partial^2 J}{\partial X^2}. \quad (37)$$

Notice that J is locally conserved, and the following integral conservation identity holds:

$$1 = -[S]_{-\infty}^{\infty} = - \int_{-\infty}^{\infty} \frac{\partial S}{\partial X} dX = \int_{-\infty}^{\infty} J dX. \quad (38)$$

Eq. (37) has Gaussian solutions satisfying (38),

$$J(X, T) = \frac{1}{2\sqrt{\pi A(T)}} \exp \left[-\frac{X^2}{4 A(T)} \right], \quad (39)$$

which yields

$$S(X, T) = \frac{1}{2} \operatorname{erfc} \left[\frac{X}{2\sqrt{A(T)}} \right] \quad (40)$$

for the wave front profile [12]. Inserting Eq. (39) in Eq. (37), we find the following equation for $A(T) > 0$:

$$\frac{dA}{dT} - 2U'(K) A = D(K). \quad (41)$$

After insertion of (39), the flux (36) becomes

$$\frac{j_k}{j_\infty} \sim \sqrt{\frac{3}{2A\tilde{\varphi}}} K^{2/3} \exp \left\{ \frac{\tilde{\varphi}}{2\epsilon^3} - \frac{G(K)}{\epsilon^3} - \frac{G'(K)X}{\epsilon^{3/2}} - \frac{G'(K)}{2} - \left[\frac{G''(K)}{2} + \frac{1}{4A} \right] X^2 \right\}, \quad (42)$$

$$j_\infty = \sqrt{\frac{\tilde{\varphi}}{6\pi\epsilon}} \exp \left(-\frac{\tilde{\varphi}}{2\epsilon^3} + \frac{3\tilde{\varphi}}{2\epsilon} \right). \quad (43)$$

Here $K = K(T)$ and $A = A(T)$ are found by solving the differential equations (31) and (41) with initial conditions $K(0) = \epsilon^3$ and $A(0) = 3\epsilon^4/(2\tilde{\varphi})$, respectively. Eq. (43) is the classical Zeldovich quasi-steady nucleation rate of supercritical clusters, and it can be directly obtained from the stationary flux (26) in the limit as $\epsilon \rightarrow 0$.

C. The nucleation rate of supercritical clusters

Let us now study the transient creation rate, in which $j \equiv j_{k_c}$ increases from 0 to the steady Zeldovich value (43). As we have just seen, our theory predicts that *the wave front*

profile is given by (40), where $K(T)$ and $A(T)$ are solutions of Eqs. (31) and (41), respectively. The flux of clusters with sizes larger than k is then given by Eq. (42). Setting $k = k_c = \epsilon^{-3}$ (critical size) and $X = (1 - K(T))/\epsilon^{3/2}$ in this equation, we obtain the nucleation rate predicted by our theory, $j(t)$. Its integral over time yields the number of supercritical clusters, $N_c(t)$. We shall consider now a different and more explicit approximation of these results: We linearize the wave front equation (31) about the critical size $K = 1$ and insert the solution into (42).

1. *Linearization of the wave front speed about the critical size*

Let us fix $k = k_c = \epsilon^{-3}$ (critical size) in the definition (33) of X :

$$X = \frac{1 - K}{\epsilon^{3/2}} \equiv \kappa. \quad (44)$$

We now set $X = \kappa$ in (42) and perform the limit as $\epsilon \rightarrow 0$ with κ fixed. The result is

$$j \sim j_\infty e^{-\tilde{\varphi}\kappa^2/6 - \epsilon^{3/2}\tilde{\varphi}\kappa/6} \sim j_\infty e^{-\tilde{\varphi}\kappa^2/6}, \quad (45)$$

provided we use the limiting stationary value $(4A)^{-1} = -G''(1)/2$.

The transient turns on when $\kappa \equiv (1 - K)/\epsilon^{3/2} = O(1)$. Since $U(1 - \epsilon^{3/2}\kappa) \sim \epsilon^{3/2}\tilde{\varphi}\kappa/3$, the wave front equation (31) yields

$$\frac{d\kappa}{dT} = -\frac{\tilde{\varphi}}{3}\kappa, \quad (46)$$

as $\epsilon \rightarrow 0$. The solution of this equation is

$$\kappa = \kappa_M e^{-\tilde{\varphi}e^{\tilde{\varphi}}(T-T_M)/3} = \kappa_M e^{-(t-t_M)/(2\tau)}, \quad (47)$$

$$\tau^{-1} = \frac{2}{3}\tilde{\varphi}\epsilon. \quad (48)$$

We select κ_M as the value at which the flux j reaches its inflection point. Then we may consider that the wave front has ignited the nucleation of supercritical clusters. Straightforward use of Eqs. (45) and (46) shows that

$$\kappa_M = \sqrt{\frac{6}{\tilde{\varphi}}}. \quad (49)$$

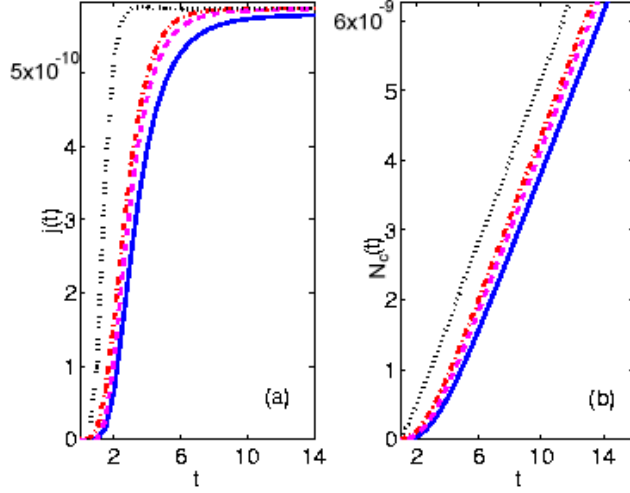


FIG. 2: (a) Evolution of the dimensionless flux at critical size $j(t)$, and (b) number of clusters surpassing critical size $N_c(t)$ as a function of dimensionless time for disilicate glass at 703K, $k_c = 18$. Solid lines correspond to numerical results, dashed lines to the approximation given by Eq. (42), dot-dashed lines to the linearization approximation (50) and dotted lines to linearizing the equations for $K(T)$ and $A(T)$ as in Appendix C of Ref. [12].

Moreover, $T_M = \epsilon t_M$ is the *time to ignition*, at which the wave front $K(T)$ reaches the value $K = 1 - \epsilon^{3/2}\kappa_M$. From (31), we obtain t_M and from (45) and (47), we obtain the flux [12]

$$\begin{aligned}
 j &\sim j_\infty e^{-(t-t_M)/\tau}, & (50) \\
 t_M &= t_\infty + \frac{3}{2\tilde{\varphi}\epsilon} \left\{ \ln \left(\frac{\tilde{\varphi}(1-\epsilon^3)^2}{6\epsilon^3} \right) \right. \\
 &\quad \left. + \int_{\epsilon^3}^{1-\epsilon^{3/2}\kappa_M} \left[\frac{\tilde{\varphi}}{3K^{2/3} \sinh \left[\frac{\tilde{\varphi}}{2}(K^{-1/3} - 1) \right]} + \frac{2}{K-1} \right] dK \right\}. & (51)
 \end{aligned}$$

Here t_∞ is the duration of the initial stage. Integrating $j(t)$ over time, we find the number of supercritical clusters as a function of time. In the limit as $t \rightarrow \infty$, this number is $N_c(t) \sim j_\infty (t - \theta)$, where the time lag θ is approximately given by $\theta = t_M + \tau\gamma + \tau E_1(e^{t_M/\tau})$, in which $\gamma = 0.577215\dots$ is Euler's constant and $E_1(x)$ is an exponential integral, see the derivation in Appendix B of Ref. [12]. The time lag θ can be directly compared to experimental values [3].

2. Comparison between different approximations

Fig. 2(a) compares $j(t)$ calculated from the numerical solution of the BDE for devitrification of disilicate glass at 703 K, from (50) and (51) with $t_\infty = 0$, and from Eq. (42) with $X = (1 - K(T))/\epsilon^{3/2}$. We find that the more precise expression, Eq. (42), captures better the width and location of the transition region between $j = 0$ and $j = j_\infty$, as compared with the simple approximation given by Eqs. (50) and (51). Both approximations present a small overshoot and yield a smaller time lag θ than that obtained from the numerical solution of the BDE. The overshoot decreases as the critical size increases. Another approximation consists of linearizing the equations for $K(T)$ and $A(T)$ about the critical size $K = 1$ as suggested in Ref. [15]. This latter approximation is the worst one. This is not surprising as such approximation provides the same result for both the discrete BDE and the continuum ZFE.

For disilicate glass at a lower temperature of 703 K, the critical size is smaller and our approximations deviate more from the numerical solution of the BDE, as shown in Figure 2(a). Integrating $j(T)$ over time, we find the number of supercritical clusters as a function of time, $N_c(t)$, which is depicted in Figs. 2(b). The numerical solution of the BDE with the TF diffusivity yields a time lag $\theta = 2.6$. This value is close to those provided by the linearization approximation, $\theta = 2.2$, and by Eq. (42), $\theta = 2.3$. Thus these analytical approximations to the numerical solution are reasonably good even for a relatively small critical size. However, $\theta = 2.6$ gives 3.2 hours according to Table I, whereas the experimentally measured time lag is about 50 hours, cf. Fig. 5 of Ref. [3]. This discrepancy is due to having used the TF discrete diffusivity, which yields an excessively small time unit, as shown in Table I.

IV. MODIFIED MODEL OF NUCLEATION AND GROWTH

It is somewhat paradoxical that the TF discrete diffusivity is proportional to $k^{2/3}$ (cluster area), whereas growth stages of a cluster after nucleation are due to diffusive accretion of monomers which yields a discrete diffusivity proportional to $k^{1/3}$ (cluster radius). In this section, we propose a model that interpolates between these two mechanisms and produces a discrete diffusivity proportional to $k^{2/3}$ for small cluster size and proportional to $k^{1/3}$ for large cluster size. The idea is to consider that the discrete diffusivity should be consistent

with adiabatic growth of a large cluster at whose surface the concentration of monomers is different from the monomer concentration at infinity. We then modify the Becker-Döring equations to accomodate the resulting law for cluster growth [16].

A. Modified Becker-Döring model

To be precise, consider a spherical k -cluster which is growing adiabatically by diffusion of monomers across its interface. If the diffusion coefficient is approximately constant, the concentration solves Laplace's equation in spherical coordinates with densities ρ_a at the sphere radius $r = a$, and ρ_∞ at infinity:

$$\rho(r) = \rho_\infty + \frac{\rho_a - \rho_\infty}{r} a. \quad (52)$$

Suppose now that the crystal particles occupy all available sites inside the cluster, whereas they occupy the volume fraction ρ outside the cluster. Then the number of molecules falling into the cluster surface per unit time is $(1 - \rho)4\pi a^2(da/dt)/v$, and this number should equal the diffusive flux times the cluster surface area:

$$\frac{4\pi a^2 D}{v} \frac{\partial \rho}{\partial r}(a) = (1 - \rho) \frac{4\pi a^2}{v} \frac{da}{dt^*}. \quad (53)$$

This implies

$$\frac{dk}{dt^*} = \frac{(\rho_\infty - \rho_a) 4\pi a D}{(1 - \rho) v} = \frac{(\rho_\infty - \rho_a) (4\pi)^{2/3} D (3k)^{1/3}}{(1 - \rho) v^{2/3}}. \quad (54)$$

Using now (A9) for large, near-critical cluster sizes,

$$\frac{dk}{dt^*} \sim -\frac{12Dk^{2/3}D_+g_k}{v^{2/3}} \sim -12D(k/v)^{2/3}(\sigma k^{-1/3} - \varphi_a), \quad (55)$$

in which φ_a is the free energy per molecule at the cluster radius. Similarly, $\rho_\infty - \rho_a \sim \tilde{\varphi} - \varphi_a$ if the free energy per molecule is small, and Equations (54) and (55) yield

$$\varphi_a - \sigma k^{-1/3} \sim \frac{(\pi/6)^{2/3}(\tilde{\varphi} - \varphi_a)}{(1 - \rho) k^{1/3}} \implies \varphi_a \sim \frac{\tilde{\varphi}(1 + \mu)}{\mu + \epsilon k^{1/3}}. \quad (56)$$

Here we have used (28) and the definition

$$\mu = \frac{\epsilon(\pi/6)^{2/3}}{1 - \rho}. \quad (57)$$

Equations (28), (55) and (57) provide

$$\frac{dk}{dt^*} \sim -\Omega k^{2/3} \frac{\tilde{\varphi}[(\epsilon k^{1/3})^{-1} - 1]}{1 + \epsilon k^{1/3}/\mu}, \quad (58)$$

in which Ω is as defined in (6).

Equation (58) describes the diffusive growth of a crystal nucleus in a glass phase such that the concentration at the interface is different from that at infinity. We shall now modify the BDE in such a way that the same equation is obtained in the limit of large clusters near critical conditions. We shall replace the BD flux (2) by:

$$j_k = (e^{-D+g_k+\Psi_k} \rho_k - \rho_{k+1}) d_k, \quad (59)$$

which is equivalent to replacing $\rho_1 e^{\Psi_k}$ instead of the monomer density in (2). We shall now select Ψ_k so that the new drift velocity

$$v_k = (e^{-D+g_k+\Psi_k} - 1) d_k, \quad (60)$$

becomes

$$v_k \sim -k^{2/3} \frac{D+g_k}{1 + \epsilon k^{1/3}/\mu}, \quad (61)$$

in the limit of large, near critical cluster sizes. Writing time in dimensional units, Eq. (61) is (58) up to higher order terms. From (6) and (60), we obtain $v_k \sim -k^{2/3} (\Psi_k - D+g_k)$, which compared to (61) yields

$$\Psi_k = \epsilon k^{1/3} \frac{D+g_k}{\mu + \epsilon k^{1/3}}. \quad (62)$$

The modified BDE are therefore (1) with the flux (59) and (62) together with the mass constraint (4).

B. Equilibrium and stationary solution

Our modified BDE do not have a Gibbsian equilibrium (8) nor satisfy detailed balance. Instead, the equilibrium distribution for which $j_k = 0$ is

$$\tilde{\rho}_k = \exp \left(-g_k + \sum_{j=1}^{k-1} \Psi_j \right). \quad (63)$$

As before, it is convenient to define a new distribution s_k which is 1 at equilibrium:

$$\rho_k = \exp\left(-\alpha + k\varphi - \sigma_k + \sum_{j=1}^{k-1} \Psi_j\right) s_k, \quad (64)$$

for $k = 2, 3, \dots$ and $s_1 \equiv 1$. In terms of s_k , the flux (59) becomes

$$j_k = -d_k \exp\left(-\alpha + (k+1)\varphi - \sigma_{k+1} + \sum_{j=1}^k \Psi_j\right) (s_{k+1} - s_k). \quad (65)$$

The stationary solution satisfies the equation $j_k = e^{-\alpha} j_\infty$, with constant flux j_∞ . The result is

$$s_k = 1 - j_\infty \sum_{l=1}^{k-1} \exp\left(\sigma_{l+1} - (l+1)\varphi - \sum_{j=1}^l \Psi_j - \ln d_l\right). \quad (66)$$

Since $s_k \rightarrow 0$ as $k \rightarrow \infty$, we obtain the stationary flux

$$j_\infty = \frac{1}{\sum_{l=1}^{\infty} \exp[\sigma_{l+1} - (l+1)\varphi - \sum_{j=1}^l \Psi_j - \ln d_l]}. \quad (67)$$

C. Numerical results

In terms of the s_k , the BDE are

$$\dot{s}_k + u_k(s_{k+1} - s_k) = -\left(k\dot{\varphi} + \sum_{j=1}^{k-1} \dot{\Psi}_j\right) s_k + d_{k-1}(s_{k-1} - 2s_k + s_{k+1}), \quad (68)$$

for $k \geq 2$ and $s_1 \equiv 1$. Here the new advection velocity is

$$u_k = d_{k-1} - d_k e^{\varphi - D + \sigma_k + \Psi_k}. \quad (69)$$

We have to solve the BDE with initial condition $s_k(0) = 0$ for $k \geq 2$. The mass constraint (21) is now

$$e^{\varphi(0)} = e^\varphi + \sum_{k=2}^{\infty} k e^{k\varphi - \sigma_k + \sum_{j=1}^{k-1} \Psi_j} s_k. \quad (70)$$

In (62), the parameter μ can be written as

$$\mu = \frac{\epsilon (\pi/6)^{2/3}}{1 - e^{\varphi(0) - \alpha}}, \quad (71)$$

because $\rho = \exp[\varphi(0) - \alpha]$.

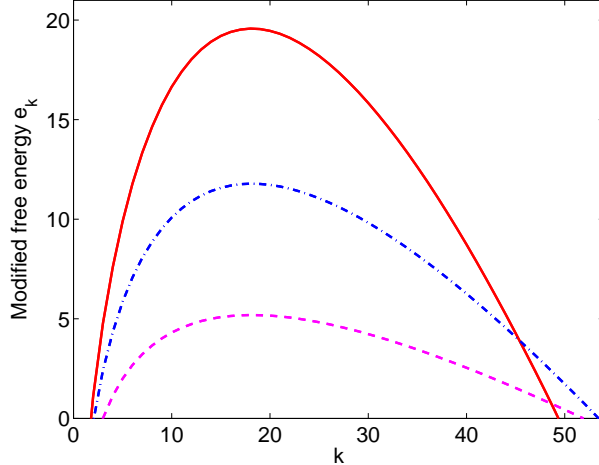


FIG. 3: Modified free energy $e_k = g_k - \sum_{j=1}^{k-1} \Psi_j - \alpha$ as a function of the size k for $\mu = 10$ (solid line), $\mu = 1$ (dot-dashed line) and $\mu = 1/3$ (dashed line).

As indicated previously, with the initial condition of pure monomers φ rapidly evolves to a quasistationary value $\tilde{\varphi}$ and a continuum size distribution emerges. We have to select the initial chemical driving force $\varphi(0)$ so that the quasistationary value $\tilde{\varphi}$ given by Eq. (16) is attained at the end of the initial stage. Notice that $\varphi(0)$ enters the definition (71) and the constraint (70). Not knowing the monomer-monomer bonding energy α , we find easier to fix μ at different values and find $\varphi(0)$ in (70) so that the quasistationary value $\tilde{\varphi}$ of Eq. (16) is attained at the end of the initial stage. The limit as $\mu \rightarrow \infty$ gives us back the original BDE with the TF discrete diffusivity.

We have solved the modified BD model with parameter values corresponding to disilicate glass at $T = 703\text{K}$ ($k_c = 18$) in Table I for three values $\mu = 10, 1, 1/3$. The corresponding modified free energy $e_k = g_k - \sum_{j=1}^{k-1} \Psi_j - \alpha$ is depicted in Fig. 3. We observe that the energy barrier becomes flatter as μ decreases and the departure from the usual BDE with TF discrete diffusivity is greater. Fig. 4(a) shows the evolution of the size distribution function $s_k(t)$ towards its stationary profile when $\mu = 1$. Comparison between the three stationary profiles of the size distribution function is depicted in Fig. 4(b). Notice that the profiles for $\mu = 1$ and $\mu = 1/3$ almost coincide and are noticeably less steep than the profile for $\mu = 10$.

The size distribution function s_k has a step-like profile whose inflection point marks the

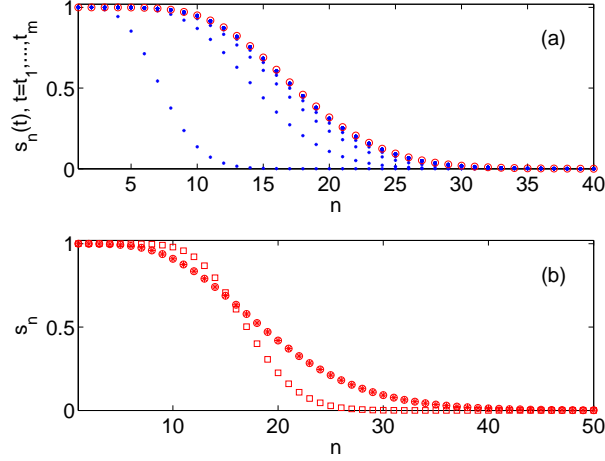


FIG. 4: (a) Profiles of s_k for $\mu = 1$ at different times. The profile of the stationary size distribution function is indicated by circles. (b) Stationary profiles of the size distribution function for $\mu = 10$ (squares), $\mu = 1$ (circles) and $\mu = 1/3$ (dots).

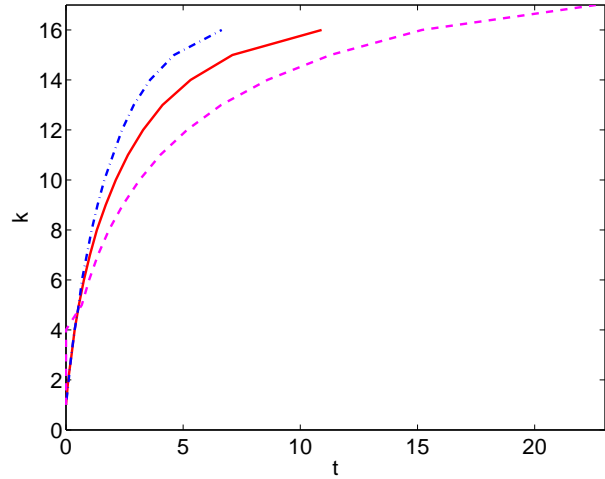


FIG. 5: Evolution of the wave front position towards the critical size $k_c = 18$ for $\mu = 10$ (dot-dashed line), $\mu = 1$ (solid line) and $\mu = 1/3$ (dashed line).

instantaneous location of the wave front advancing in size space. Fig. 5 shows the evolution of the wave front location. We observe that the velocity of the wave front decreases as μ decreases.

Lastly, we have calculated the evolution of the flux at critical size and the number of

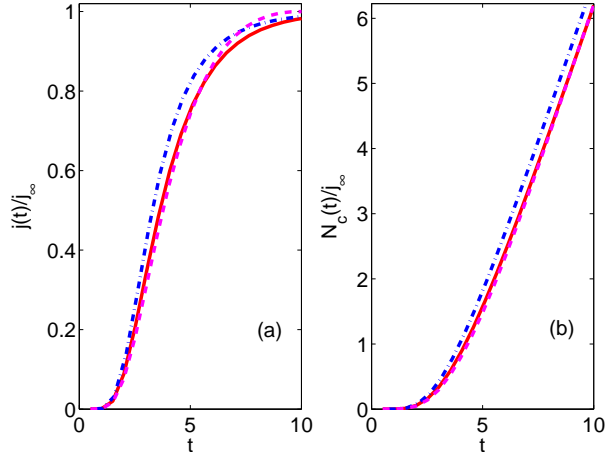


FIG. 6: (a) Evolution of the normalized flux at critical size, $j(t)/j_\infty$, and (b) number of clusters surpassing critical size, $N_c(t)$, for disilicate glass at 703 K and $\mu = 10$ (dot-dashed line), $\mu = 1$ (solid line) and $\mu = 1/3$ (dashed line). Time lags are 2, 2.2 and 2.3, respectively.

supercritical clusters for $\mu = 10, 1, 1/3$; see Fig. 6. For these values of μ , we have found $\varphi(0) = 4.79, 6.9, 21.8$ and $j_\infty = 2.1 \times 10^{-9}, 4.1 \times 10^{-6}, 2.8 \times 10^{-3}$, respectively.

V. DISCUSSION

In this paper, we have studied the case of phase segregation resulting when $\rho > \rho_c$. Previously, other authors had carried out asymptotic studies of the BDE in the simpler case of subcritical density, $\rho < \rho_c$, in which initial conditions of only monomers, or more general ones, evolve towards the equilibrium distribution. In many cases of polynomial growth for d_k , equilibrium is reached via a wave front profile for s_k , which is similar to Eq. (40) with $A \propto K^\delta$, and $K \propto T^\mu$, for appropriate positive δ and μ ; see Ref. [17] and references cited therein. This advancing and widening wave front leaves in its wake the equilibrium size distribution.

In the more complex present case of phase segregation and indefinite aggregate growth, a quasicontinuum wave front of s_k emerges after a short transient which is governed by the discrete BDE. After this, the leading edge of the wave front advances towards the critical size, and it slows down and stops there, leaving behind it a quasi-equilibrium state. The arrival of the wave front to the critical size marks the *ignition* of nucleation of supercritical

clusters, which ends when the stationary Zeldovich rate is reached. Previous asymptotic theories (see [15, 18, 19, 20, 21, 22] and references cited therein) have been derived for the continuum ZFE, not the discrete BDE, and thus their results systematically misrepresent two things: (i) the time lags for transient nucleation, as explained by Wu [9], and (ii) the width of the wave front and the time to ignition in the nucleation rate. The latter discrepancies occur because the diffusion coefficient appearing in the continuum equation for the wave front satisfies $D_{BDE}(K) = D_{ZFE}(K) - U(K)/2$, and therefore the time to ignition in the nucleation rate for the BDE is *smaller* than the corresponding one for the ZFE.

Let us briefly mention several existing asymptotic theories for the ZFE. Shneidman [19] and Shi et al [20] Laplace transformed the continuum ZFE and matched a first stage of pure advection of clusters to a local expansion about the wave front when it is near its final position at the critical size. They obtained our simplest formula for the nucleation rate, Eq. (50) with the same relaxation time, τ_{TF} or τ_{TDG} , except that their values for t_M were different from (51). This can be expected from Wu's arguments about approximating the discrete BDE by the continuum ZFE [9]; see the systematic shift of approximations of the ZFE with respect to numerical solutions of the BDE in Fig. 20 of Ref. [9]. Trinkaus and Yoo [18] studied a ZFE with a drift term linearized about the critical size (parabolic barrier) as an approximation to the full ZFE. Their results are comparable to those found by means of the Laplace transform and matched asymptotic expansions; see Wu's review [9]. All these authors obtained a transition region for the nucleation rate $j(t)$ that was wider than observed in the numerical solution of the BDE. Several authors also found a nucleation rate for supercritical clusters that did not tend to j_∞ as $t \rightarrow \infty$ if $k \neq k_c$ [15, 18, 20], which is often called the *asymptotics catastrophe* [21]. Our theory is free from this deficiency [12]. Shneidman [22] criticized Maksimov et al's result and extended his earlier asymptotic formula for the nucleation rate [23] to non-critical sizes. The previous criticism of using approximations to the ZFE instead of approximations to the discrete BDE apply to these works. Our more precise approximation using Eq. (42) plus the exact equations for the wave front location and its instantaneous width improve upon other approximations and perform better for materials with large critical sizes.

The time lag obtained from the numerical solution of the BDE with the TF diffusivity (or from our asymptotic approximations using it) is too small as compared with experimental results (about fifteen times smaller for disilicate at 703 K). The TF discrete diffusivity yields

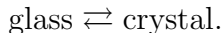
an excessively small time unit, as shown in Table I. Another difficulty is that the TF d_k is proportional to the surface area of the k cluster whereas diffusive growth of a cluster after the nucleation has ceased produces $d_k \propto k^{1/3}$, as in late stage coarsening theories [8]. We have proposed a new modification of the BDE that yields a size advection velocity proportional to $k^{2/3}D_+g_k$ for small k , and to $k^{1/3}D_+g_k$ for large k , thereby interpolating between TF and diffusive growth formulas. With the new modification, time lags are somewhat larger, but j_∞ increases unrealistically because the effective activation energy barrier diminishes. The usual way to improve agreement with experiments is to change the surface tension so that j_∞ agrees with measurements. It is clear that we should optimize the choice of the surface tension and of the monomer-monomer bonding energy α to assess the merits of our proposal. Lastly, the flatness of the activation energy barrier for small μ as depicted in Fig. 3 indicates that expansions about the barrier maximum will provide poor approximations and that the corresponding asymptotic theory for our modified BDE may not be an immediate extension of our results for the classical BDE.

Acknowledgments

The present work was financed by the Spanish MCyT grants BFM2002-04127-C02-01 and BFM2002-04127-C02-02, by the Spanish MECD grants MAT2005-05730-C02-01 and MAT2005-05730-C02-01, and by the European Union under grant HPRN-CT-2002-00282.

APPENDIX A: TURNBULL-FISHER DISCRETE DIFFUSIVITY

To derive d_k for a glass-crystal transformation, we assume that the particles at the glass-crystal interface are undergoing reactions



The forward and backward reactions have activation energies ε_+ and ε_- : During the conversion of one glass particle to crystal, one has to climb up one side of an energy barrier with height ε_+ , and then descend an energy ε_- . The net free energy change should equal the chemical potential:

$$\frac{\varepsilon_+ - \varepsilon_-}{k_B T} = D_+ g_k. \tag{A1}$$

The forward and backward rate constants of the reactions are

$$\kappa_+ = \beta e^{-\frac{\varepsilon_+}{k_B T}}, \quad \kappa_- = \beta e^{-\frac{\varepsilon_-}{k_B T}}, \quad (\text{A2})$$

respectively. Here β is a positive constant. The kinetic rate constants can be rewritten as

$$\kappa_+ = \beta e^{-\frac{Q}{RT}} e^{-D_+ g_k/2}, \quad \kappa_- = \beta e^{-\frac{Q}{RT}} e^{D_+ g_k/2}, \quad (\text{A3})$$

provided $Q/N_A = (\varepsilon_+ + \varepsilon_-)/2$ is the mean barrier height. The common prefactor $\beta e^{-Q/RT}$ is the inverse time constant of the reactions when $D_+ g_k = 0$ and neither phase is formed. For a spherical cluster with k monomers, this prefactor is the molecular jump rate at the cluster surface, which may coincide with the rate of molecular diffusion in the glass phase. Since a glass particle must push aside other glass particles when it moves, it is plausible that molecular diffusion in the glass phase is an activated process, as suggested by (A3). The diffusion coefficient D is one third the mean velocity times the mean free path $\lambda \approx v^{1/3}$ according to elementary kinetic theory. Then the diffusion jump rate is $3D/\lambda^2$, and we can identify

$$\beta e^{-\frac{Q}{RT}} = \frac{3D}{v^{2/3}}, \quad \text{i.e.,} \quad \beta = \frac{3D_0}{v^{2/3}}, \quad D = D_0 e^{-\frac{Q}{RT}}. \quad (\text{A4})$$

Consider now the growth of a k -cluster by converting glass particles to the crystal phase in the active sites at its interface. Individual conversions are discrete events whose time sequence is a Poisson process. Let k_+ be the number of glass to crystal conversions happening on the cluster interface in a short time δt^* . The expected value of k_+ is the number of active sites at the cluster interface times the number of glass to crystal conversions $\kappa_+ \delta t^*$. The number of active sites is the area of the spherical k -cluster of radius $[3kv/(4\pi)]^{1/3}$ divided by the area a single molecule would occupy on the cluster interface, namely, $\pi[3v/(4\pi)]^{2/3}$. Then, $\mathcal{A}_k = 4k^{2/3}$ and $\langle k_+ \rangle$ satisfies

$$\langle k_+ \rangle = \mathcal{A}_k \kappa_+ \delta t^*, \quad \langle (k_+ - \langle k_+ \rangle)^2 \rangle = \langle k_+ \rangle = \mathcal{A}_k \kappa_+ \delta t^*. \quad (\text{A5})$$

The conversions from crystal to glass are another Poisson process for which

$$\langle k_- \rangle = \mathcal{A}_k \kappa_- \delta t^*, \quad \langle (k_- - \langle k_- \rangle)^2 \rangle = \langle k_- \rangle = \mathcal{A}_k \kappa_- \delta t^*. \quad (\text{A6})$$

We assume that the backward and forward Poisson processes are independent, so

$$\langle (k_+ - \langle k_+ \rangle)(k_- - \langle k_- \rangle) \rangle = 0. \quad (\text{A7})$$

Equations (A5) to (A7) imply that the net number of glass-crystal conversions, $\delta k \equiv k_+ - k_-$, has the statistics

$$\langle \delta k \rangle = \mathcal{A}_k(\kappa_+ - \kappa_-) \delta t^*, \quad \langle (\delta k - \langle \delta k \rangle)^2 \rangle = \mathcal{A}_k(\kappa_+ + \kappa_-) \delta t^*. \quad (\text{A8})$$

Inserting (A3) and (A4) into these equations, we obtain

$$\langle \delta k \rangle = \frac{24k^{2/3}D}{v^{2/3}} \sinh\left(\frac{-D+g_k}{2}\right) \delta t^*, \quad \langle (\delta k - \langle \delta k \rangle)^2 \rangle = \frac{24k^{2/3}D}{v^{2/3}} \cosh\left(\frac{D+g_k}{2}\right) \delta t^*. \quad (\text{A9})$$

We now identify the velocity $v_k = (e^{-D+g_k} - 1) d_k$ in the BDE with $\Omega^{-1} \delta \langle k \rangle / \delta t^*$, and this yields the diffusivity (6). Eq. (A9) also provides the diffusion coefficient (35).

-
- [*] E-address `bonilla@ing.uc3m.es`. Author to whom all correspondence should be addressed.
- [†] E-address `ana_carpio@mat.ucm.es`.
- [‡] E-address `jfarjoun@math.berkeley.edu`.
- [◇] E-address `neu@math.berkeley.edu`.
- [1] E.M. Lifshitz and L.P. Pitaevskii, *Physical Kinetics*, (Pergamon Press, New York, 1981).
- [2] K. F. Kelton, A. L. Greer and C. V. Thompson, Transient nucleation in condensed systems. *J. Chem. Phys.* **79**, 6261-6276 (1983).
- [3] K. F. Kelton, Crystal nucleation in liquids and glasses, in *Solid State Physics, Vol. 45*, edited by H. Ehrenreich and D. Turnbull, pages 75-177, (Academic Press, New York, 1991).
- [4] V. Capasso, ed. *Mathematical Modelling for Polymer Processing*. Mathematics in Industry **2**. (Springer, Berlin 2003).
- [5] J.N. Israelachvili, *Intermolecular and Surface Forces*, 2nd. ed. (Academic Press, New York, 1991).
- [6] J. C. Neu, J. A. Cañizo and L. L. Bonilla, Three eras of micellization. *Phys. Rev. E* **66**, 061406 (2002) (9 pages).
- [7] B. Niethammer, On the evolution of large clusters in the Becker-Döring Model. *J. Nonlin. Sci.* **13** 115-155 (2003).
- [8] I. M. Lifshitz and V. V. Slyozov, The kinetics of precipitation from supersaturated solid solutions. *J. Phys. Chem. Solids* **19**, 35-50 (1961).
- [9] D. T. Wu, Nucleation theory. *Solid State Physics 50: Advances in Research and Applications*, edited by H. Ehrenreich and F. Spaepen. Academic P., San Diego. Pp. 37-187 (1996).

- [10] A. Hammond and F. Rezakhanlou, The kinetic limit of a system of coagulating Brownian particles. LANL preprint archive, math.PR/0408395 (68 pages).
- [11] O. Penrose and A. Buhagiar, Kinetics of nucleation in a lattice gas model: microscopic theory and simulation compared. *J. Stat. Phys.* **30**, 219-241 (1983).
- [12] J. C. Neu, L. L. Bonilla and A. Carpio, Igniting homogeneous nucleation. *Phys. Rev. E* **71**, 021601 (2005) (14 pages).
- [13] J. M. Ball, J. Carr and O. Penrose, The Becker-Döring cluster equations: basic properties and asymptotic behavior of solutions. *Comm. Math. Phys.* **104**, 657-692 (1986).
- [14] O. Penrose, The Becker-Döring equations at large times and their connection with the LSW theory of coarsening. *J. Stat. Phys.* **89**, 305-320 (1997).
- [15] P. Demo and Z. Kozísek, Homogeneous nucleation processes: Analytical approach. *Phys. Rev. B* **48**, 3620-3625 (1993).
- [16] This Section is based on Y. Farjoun's Ph.D. thesis.
- [17] J.R. King and J.A.D. Wattis, Asymptotic solutions of the Becker-Döring equations with size-dependent rate constants. *J. Phys. A* **35**, 1357-1380 (2002).
- [18] H. Trinkaus and M. H. Yoo, Nucleation under time-dependent supersaturation. *Phil. Mag. A* **55**, 269-289 (1987).
- [19] V. A. Shneidman, Size distribution of new-phase particles during transient condensation of a supercooled gas. *Zh. Tekh. Fiz.* **57**, 131-140 (1987) [*Sov. Phys. – Tech. Phys.* **32**, 76-81 (1987)].
- [20] G. Shi, J. H. Seinfeld and K. Okuyama, Transient kinetics of nucleation. *Phys. Rev. A* **41**, 2101-2108 (1990).
- [21] I. L. Maksimov, M. Sanada and K. Nishioka, Energy barrier effect on transient nucleation kinetics: Nucleation flux and lag-time calculation. *J. Chem. Phys.* **113**, 3323-3331 (2000).
- [22] V. A. Shneidman, Transient nucleation distributions and fluxes at intermediate times and sizes. *J. Chem. Phys.* **115**, 8141-8151 (2001).
- [23] V. A. Shneidman, Transient critical flux in nucleation theory. *Phys. Rev. A* **44**, 2609-2611 (1991).